Journal of Environmental Monitoring

Cite this: *J. Environ. Monit.*, 2012, **14**, 1684

www.rsc.org/jem

PAPER

Insights into ozone deposition patterns from decade-long ozone flux measurements over a mixed temperate forest†

J. Neirynck,*[a] B. Gielen,[b] I. A. Janssens[b] and R. Ceulemans[b]

Received 21st November 2011, Accepted 23rd March 2012
DOI: 10.1039/c2em10937a

Long-term fluxes of ozone (O_3) were measured over a mixed temperate forest using the aerodynamic gradient method. The long-term average O_3 flux (F) was -366 ng m^{-2} s^{-1} for the period 2000–2010, corresponding to an average O_3 concentration of 48 μg m^{-3} and a deposition velocity v_d of 9 mm s^{-1}. Average nocturnal ozone deposition amounted to -190 ng m^{-2} s^{-1}, which was about one third of the daytime flux. Also during the winter period substantial O_3 deposition was measured. In addition, total O_3 fluxes were found to differ significantly among canopy wetness categories. During the day, highest deposition fluxes were generally measured for a dry canopy, whereas a rain-wetted canopy constituted the best sink at night. Flux partitioning calculations revealed that the stomatal flux (F_s) contributed 20% to the total F but the F_s/F fraction was subject to seasonal and diurnal changes. The annual concentration-based index AOT40 (accumulated dose over a threshold of 40 ppb) and the Phytotoxic Ozone Dose (POD_1 or accumulated stomatal flux above a threshold of 1 nmol m^{-2} s^{-1}) were related in a curvilinear way. The O_3 deposition was found to be largely controlled by non-stomatal sinks, whose strength was enhanced by high friction velocities (u_*), optimizing the mechanical mixing of O_3 into the canopy and the trunk space. The long-term geometrical mean of the non-stomatal resistance (R_{ns}) was 136 s m^{-1} but lower R_{ns} values were encountered during the winter half-year due to higher u_*. The R_{ns} was also subject to a marked diurnal variability, with low R_{ns} in the morning hours, when turbulence took off. We speculate that non-stomatal deposition was largely driven by scavenging of ozone by biogenic volatile organic compounds (BVOCs) and especially NO emitted from the crown or the forest floor.

Introduction

Tropospheric ozone (O_3) is a major secondary, phytotoxic air pollutant, whose complex photochemical formation is sustained by primary precursor emissions of nitrogen oxides (NO_x) and volatile organic compounds (VOCs).[1] It is also a greenhouse gas; in importance it occupies the third place behind CO_2 and CH_4 (IPCC, 2007). Tropospheric O_3 has deleterious effects on human health (WHO, 2003) and is harmful for crop production and forest vitality in many regions of the Northern Hemisphere.[2] In a recent decadal trend analysis it was observed that O_3 displayed increasing trends at rural observation sites in North-western and Central Europe.[3] Enhanced monitoring of this pollutant in a temperate maritime climate, along with its precursors, is therefore recommended.

[a]*Research Institute for Nature and Forest, Gaverstraat 4, B-9500 Geraardsbergen, Belgium. E-mail: johan.neirynck@inbo.be; Fax: +32 (0)54 436189; Tel: +32 (0)54 437119*
[b]*Department of Biology, University of Antwerp, Universiteitsplein 1, B-2610 Wilrijk (Antwerp), Belgium*
† Presented at the COST International Conference on Ozone, Climate Change and Forests, 14-16 June 2011, Prague, Czech Republic.

Environmental impact

Data from long-term monitoring measurements of ozone fluxes over a mixed temperate forest were used to enhance the knowledge about ozone flux partitioning, flux-based ozone risk assessment calculations and impact of environmental drivers on non-stomatal ozone fluxes. Flux data collected at our site have shown that deposition is largely controlled by non-stomatal sinks, whose strength is enhanced by turbulent mixing processes in the canopy or the trunk space. Ozone deposition processes are also clearly mediated through canopy wetness. During the day, highest deposition fluxes are generally measured for a dry canopy, whereas a rain-wetted canopy constitutes the best sink at night. The exposure-based index (AOT40) is related with the flux-based index (POD_1) in a curvilinear relationship.

Long-term measurements of O_3 deposition over forest vegetation are few[4,5] but they are necessary for several reasons. First of all, the removal of O_3 from the atmosphere by deposition at the earth's surface is an important process governing the budget of O_3 in the troposphere.[6] There exist, however, important differences in air filtering properties among all natural land cover classes. Because of their aerodynamic properties, turbulent exchange rates above forests are enhanced and more pollutants can be removed on an annual basis compared to smooth vegetation.[7] Detailed long-term data about the dry deposition of O_3 over forest and terrestrial surfaces in general, will therefore be useful for improving regional oxidant models.[8]

Ozone deposition information is further required to enhance the knowledge of integrated effects of ozone stress, and other stress variables (water, nutrients,…) on forest ecosystem functioning and especially tree carbon sequestration.[9–12] Total O_3 fluxes are routinely subdivided into a non-stomatal and a stomatal component. The latter flux is used for assessing the risk of vegetation exposed to elevated ozone doses. Flux-based O_3 metrics are considered to be more valuable in assessment of O_3 risks compared to O_3 exposure indices.[13–16] Climate change and increased CO_2 levels are further expected to modify O_3 stomatal uptake patterns and their effects should be further accounted for in risk assessment models.[1,17]

In this paper we report long-term O_3 flux measurements over a temperate mixed forest. The study aims to provide robust long-term averages of dry deposition rates for relevant environmental conditions, taking into account the diurnal and seasonal variability in ozone concentrations and fluxes. Special attention is paid to the impact of canopy wetness on the O_3 deposition. In a next step, the total flux is partitioned into a stomatal and a non-stomatal part, with special attention to the role of environmental drivers of the non-stomatal fluxes. Lastly, the stomatal fluxes are used to calculate the accumulated O_3 dose, which is compared with concentration-based O_3 indices, and attention is paid to the role of the non-stomatal fluxes and its control by environmental drivers.

Experimental

Site characteristics

The forest under investigation is a mixed coniferous/deciduous forest located in the Campine region of Flanders (Belgium, 51° 18′ N, 4° 31′ E). The forest is relatively small (over 300 ha), heterogeneous, but nearly uniform in height. It is bordered to the North and West by residential areas of the town of Brasschaat at a radius of ±500 m.[18] To the South and East the forest extends over 2 km before turning into a rural, partially forested terrain. The landscape is a coastal plain, with a gentle (0.3%) slope from the NNE to SSW at a mean elevation of 16 m. The climate is temperate maritime with a mean annual temperature of 10.8 ± 0.9 °C recorded over the period 1996–2010. Annual precipitation averages 882 ± 137 mm. Winds are predominantly from the SW (>30%).

A self-supporting welded scaffolding tower was constructed to 40 m, with a 9 m^2 ground area and platforms at 9, 15, 18, 23, 31 and 39 m. The tower resides in a 2 ha Scots pine (*Pinus sylvestris* L.) stand of the forest (planting date: 1929) next to a level-II observation plot of the European ICP-Forests network (EC-UN/ECE, 1996). The measuring site was also part of the CARBOEUROPE and NITROEUROPE research networks. The stand has an open canopy with a density of 375 trees ha^{-1}, a maximum LAI of 1.5 $m^2\ m^{-2}$ and a mean height of 21 m. Height growth between 1995 and 2010 was less than 1 m, which is in line with the height growth curvature on these sandy soils. Other Scots pine stands surround (*ca.* 150 to 300 m) the measurement tower. More distant patches include both deciduous (mainly pedunculate oak (*Quercus robur* L.) planted in 1936) and coniferous species (mainly Scots pine).

The suburban forest is exposed to different pollution sources. Westerly winds bring SO_2 and soot bearing air masses, coming either from the petrochemical industry, waste processing or power plants situated in the port of Antwerp (15 km to the W). Road traffic from the adjacent residential areas and from the southerly situated E19 highway is mainly responsible for elevated concentrations of NO_x and anthropogenic VOCs at the site. In the case of (north)easterly winds, ammonia-bearing air masses, either originating from livestock facilities or manure spreading, are transported over the forest.[18] Annual concentrations of SO_2, O_3, NO_2 and NH_3, measured during the last decade, average 11, 42, 31 and 3 μg m^{-3}, respectively. Until now, no visible evidence of ozone injury to trees or herbaceous vegetation has been noticed at our site (personal communication Arthur De Haeck).

Meteorological and O_3 measurements

Measurements of atmospheric gaseous pollutants and meteorological conditions have been made at the tower since mid-1995. Meteorological data include vertical profiles of air temperature and humidity (HMP 230 dew point transmitter and PT100, Vaisala, Finland) in aspirated radiation shields at 2, 24 and 40 m, and wind speed (LISA cup anemometer, Siggelkow GMBH, Germany) at 24, 32 and 40 m. At the top of the tower, ingoing and outgoing short-wave and long-wave radiation measurements are made by a radiometer (CNR1, pyranometer/pyrgeometer, Kipp and Zonen, the Netherlands). Rainfall is registered by a tipping bucket rain gauge (NINA precipitation pulse transmitter, Siggelkow GMBH, Germany). Two leaf wetness sensors (237F, Campbell Scientific, UK) are mounted on a 3 m long boom at the 18 m platform and directed into the canopy. All meteorological sensors are sampled at 0.1 Hz and stored as half hour means on a data logger (Campbell CR1000, UK). A sonic anemometer (model SOLENT 1012R2, Gill Instruments, Lymington, UK) has been deployed on a mast above the tower, at 41 m since 1996.

Vertical profiles of O_3 concentrations were measured at two inlets above the canopy (at 24 and 40 m) using a UV photometric analyzer (period 2000–2007: model TEI 49C, Thermo Environmental Instruments, USA (detection limit: 1 ppb; precision: 0.5 ppb), later replaced by model TEI 49I, Thermo Environmental Instruments, USA (detection limit: 1 ppb; precision: 0.25 ppb). From each inlet, air is drawn through 53.5 m long Teflon sampling tubes with a flow rate of 60 l min^{-1} and led towards an air conditioned instrument shelter perched on the concrete base of the scaffolding. Prior to transport, air is filtered through 0.5 mm Teflon filter housings, which are covered with a rain shield and mounted at the end of a 1.5 m long boom. The

Teflon tubings (external diameter 9.5 mm) are wrapped with 47 mm isolated housings and heated to 35 °C using an electric heating wire. Each inlet is sampled for 5 min before switching to the next inlet using a PLC controlled valve system. An additional filter of 0.5 μm is placed before the sample inlet from the monitor. Readings of the first minute from every inlet are discarded as sample tubes need to be flushed.

Calculation of fluxes and resistances

Fluxes (F) are calculated from the Businger–Dyer flux-profile relationships:[19,20]

$$F = -K\frac{\partial[O_3]}{\partial z} \quad (1)$$

where F is the flux (deposition is defined as negative flux) obtained by multiplying the ozone gradient from the 24 and 40 m height interval and K is the turbulent diffusivity, which is calculated as:

$$K = \frac{\kappa(z-d)u_*}{\phi}. \quad (2)$$

In this formula κ (the von Karman constant) is 0.41, z is the geometric mean of the measurement heights (29.7 m), d is the zero plane displacement (17.1 m = 0.8 times the average tree height) and u_* is the friction velocity determined as the square root of the kinematic momentum flux measured by eddy covariance. In order to account for stability effects, the universal flux-profile relationships for heat transfer ($\emptyset_h$) are applied.[19] Because the concentration measurements are made in the roughness sublayer, turbulent diffusivities estimated by eqn (2) are corrected by a factor α (= 0.86) to allow for wake turbulence generated above the canopy:[21]

$$\phi_h = \begin{cases} L \le 0 & \alpha^*\left(1 - 16\dfrac{(z-d)}{L}\right)^{-1/2} \\ L > 0 & \alpha + 5\dfrac{(z-d)}{L} \end{cases} \quad (3)$$

where L is the Obukhov length[22] and $(z-d)/L$ is the dimensionless stability parameter.

The deposition velocity (v_d) is obtained from the measured flux (F) by dividing F by difference in concentration $C_{(z-d)}$ of the measured gradient at $z-d$ (geometric mean of the gradient) and the ozone concentration inside the leaves C_0:

$$v_d(z-d) = \frac{-F}{C(z-d) - C_0} = \frac{1}{R_t} = \frac{1}{R_a(z-d) + R_b + R_c} \quad (4)$$

Since ozone is destroyed by reactions with cell walls and membranes in the substomatal cavity, C_0 is assumed to be zero. The reciprocal of v_d is called the total resistance (R_t) and is defined as the sum of the aerodynamic resistance (R_a), the quasi-laminar boundary layer resistance (R_b) and the canopy resistance (R_c). The latter resistance is calculated by subtracting the atmospheric resistances R_a and R_b from the total resistance (R_t).

The aerodynamic resistance (R_a) at the measuring height ($z-d$) is calculated according to Garland:[23]

$$R_a(z-d) = \frac{1}{\kappa u_*}\left[\ln\left[\frac{z-d}{z_0}\right] - \Psi_h\left(\frac{z-d}{L}\right) + \Psi_h\left(\frac{z_0}{L}\right)\right] \quad (5)$$

where z_0 is the roughness length (1.5 m), and Ψ_h is the integrated stability correction for heat, estimated following Beljaars and Holtslag.[24]

The quasi-laminar sublayer resistance R_b is species-dependent and estimated using semi-empirical relationships presented by Hicks and colleagues:[25]

$$R_b = \frac{2}{\kappa u_*}\left(\frac{Sc}{Pr}\right)^{2/3} \quad (6)$$

where Sc and Pr are the Schmidt and Prandtl numbers, respectively.

Considering that the flux is constant along the vertical axis between the measurement height ($z-d$) and the height of the canopy concentration, we may write:

$$F = \frac{-C(z-d)}{R_a(z-d) + R_b + R_c} = \frac{-C_c}{R_c} \quad (7)$$

where C_c is the ozone concentration at canopy height, defined as the level where the flux is decomposed into a stomatal contribution F_s and a non-stomatal part F_{ns}:[13,26]

$$F = F_s + F_{ns} = \left(\frac{-C_c}{R_s}\right) + \left(\frac{-C_c}{R_{ns}}\right) \quad (8)$$

where R_s and R_{ns} are the stomatal and non-stomatal resistance, respectively, which are mounted in parallel:

$$R_c = \left[\frac{1}{R_s} + \frac{1}{R_{ns}}\right]^{-1} \quad (9)$$

The stomatal flux F_s is obtained by combining eqn (7) and (8):

$$F_s = \left(\frac{-C_c}{R_s}\right) = \frac{-R_c}{(R_a(z-d) + R_b + R_c)R_s}C(z-d) \quad (10)$$

The canopy-scale stomatal resistance ($R_s(O_3)$) is calculated from stomatal resistances for water vapour $R_s(H_2O)$:

$$R_s(O_3) = \frac{D_{H_2O}}{D_{O_3}}R_s(H_2O) \quad (11)$$

where D_{H_2O} and D_{O_3} are the diffusivities of H_2O and O_3 (D_{H_2O}/D_{O_3} is equal to 1.65). The canopy-scale stomatal resistance $R_s(H_2O)$ was obtained from a leaf physiological submodel, which operates in a process-based multi-layer canopy model.[27] The submodel combines a biochemical photosynthesis model of Farquhar[28] with a Ball–Berry–Leuning-type stomatal model.[29]

The accumulated Phytotoxic Ozone Dose (*i.e.* the accumulated stomatal flux) of O_3 above a threshold of Y (POD_Y) is calculated for the period April–September as the sum of the differences between hourly mean values of F_s and Y nmol m^{-2} s^{-1} when F_s exceeds the threshold Y (during daylight hours). The latter is set to 1 nmol m^{-2} s^{-1} (Revised ICP vegetation Mapping Manual, 2010). A stomatal flux critical level value (Cle_f) of 8 mmol m^{-2} PLA (projected leaf area) was adopted from Norway spruce (2% reduction in biomass).

The exposure-based index AOT40 (in ppb h or ppm h) is the sum of the difference between the hourly mean ozone concentration at the displacement height ($d + z_0$) and the threshold of 40 ppb for all daylight hours accumulated over the period April till September. The concentration C_{d+z_0} is calculated rearranging eqn (4):

$$C_{d+z_0} = C(z-d)(1 - R_a(z-d)v_d(z-d)) \quad (12)$$

The critical AOT40 level of forest species is currently set to 5000 ppb h connected with a yield loss of 5% (Revised ICP vegetation Mapping Manual, 2010).

Quality data checks and rejection criteria

Data were screened to exclude instrumental and measurement problems, as well as conditions precluding the use of the flux-gradient theory (constant flux layer assumption). Gradients were checked for systematic bias between the two heights during episodes of high turbulence ($u_* > 1$ m s^{-1}) for which gradients were expected to approach zero. In order to reduce the relative errors in the concentration gradients, concentrations below 1 ppb were excluded. Friction velocities below 0.1 m s^{-1} were rejected because of probable invalid flux-profile relationships. To avoid non-stationarity problems, those data were excluded for which half-hour changes in concentrations led to changes in v_d exceeding 0.01 m s^{-1} ($|(z-d)/c \times (dc/dt)| > 0.01$ m s^{-1}). Outliers in the data were removed, rejecting any deposition velocity exceeding the maximum achievable deposition rate v_{dmax} ($1/(R_a + R_b)$), by more than a factor of two. Flux data of 2003 and 2004 were not retained for further analysis because of the low amount of reliable sonic data that were available during the summer periods.

Data handling, analysis and statistics

Data on fluxes and deposition rates were stratified in order to facilitate interpretation. Data were binned according to time of the day, season and canopy wetness. The differentiation between day and night was based on the global radiation readings using a threshold of 5 W m^{-2}. Stratification according to season was made according to day of the year (DOY) (spring: DOY 61–151, summer: DOY 152–243, autumn: DOY 244–334, winter: DOY 335–60). Summer half-year is defined as the period spanning DOY 61–243.

A further differentiation subdivided canopy wetness into three broad macroscopic wetness classes:

○ Dry canopy: leaf wetness sensor = 0; absence of visible (macroscopic) wetness but thin moisture films or deliquescent particles might still occur;

○ Dew-wetted canopy: leaf wetness sensor > 0 but no important preceding rainfall;

○ Rain-wetted canopy: contained following cases:

■ Rainfall recorded by rain gauge;

■ Leaf wetness sensor > 0 due to precipitation in the preceding 4 hours (>1 mm).

When temperatures dropped below 0 °C, the above-mentioned classification was not followed (separately defined as frost conditions). Differences among wetness categories were verified using a Kruskal–Wallis test. In addition, a principal component analysis was made to unravel relationships between environmental variables and flux characteristics.

Results

Flux characteristics

After rigorously applying all rejection criteria about 104 000 half-hourly fluxes were retained for detailed analysis. The long-term average O_3 flux (F) from the selected dataset was −366 ng m^{-2} s^{-1} for the period 2000–2010 corresponding to an average O_3 concentration of 48 μg m^{-3} and a deposition velocity v_d of 9 mm s^{-1} (Fig. 1). Seven percent of the fluxes were upward and these were more prominent during the winter. Average nocturnal ozone deposition amounted to −190 ng m^{-2} s^{-1}, which was about one third of the daytime flux (Table 1 and Fig. 2B). Highest deposition fluxes were measured during spring and summer but also during winter a substantial O_3 deposition was measured. Long-term average O_3 concentrations and fluxes during spring and summer were rather similar (Table 1). Long-term average daytime and nighttime fluxes during the summer half-year amounted to −0.6 and −0.2 μg m^{-2} s^{-1}, respectively, with average daytime and nighttime O_3 concentrations of ±70 and 50 μg m^{-3}. During summer, however, the upper quartile and 90th percentiles from concentrations and fluxes were higher compared to their corresponding spring values (Fig. 2A and B). Average v_d during the summer half-year was 1.0 and 0.5 cm s^{-1}, for daytime and

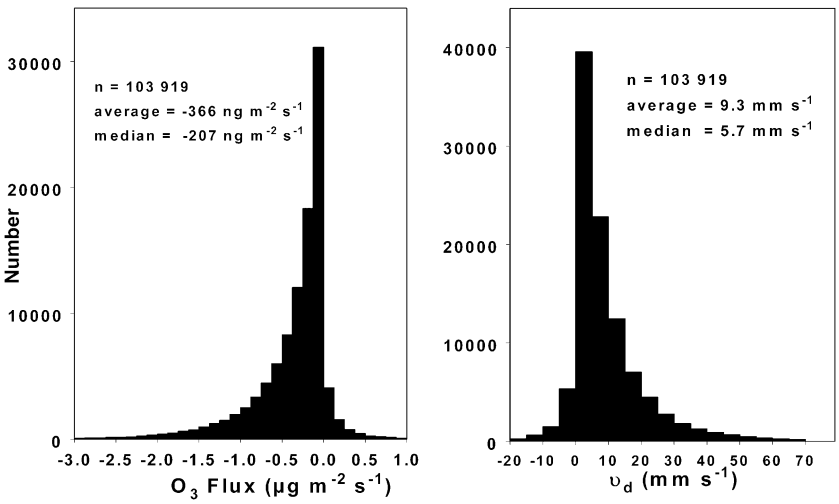

Fig. 1 Frequency distribution of half hourly ozone fluxes F (left) and deposition velocity v_d (right) for the period 2000–2010. The class width is 0.125 μg m^{-2} s^{-1} and 5 mm s^{-1} for F and v_d respectively. n = number of half-hourly flux data.

Table 1 Summary of long-term arithmetic average/median (μ_a/μ_m) O_3 concentration, flux (F) and deposition velocity (v_d) for different canopy wetness categories and time of day across the 4 seasons (spring: DOY 61–151, summer: DOY 152–243, autumn: DOY 244–334, winter: DOY 335–60). n = number of data points

		Daytime				Nighttime			
		n	O_3 (μg m^{-3})	F (ng m^{-2} s^{-1})	v_d (cm s^{-1})	n	O_3 (μg m^{-3})	F (ng m^{-2} s^{-1})	v_d (cm s^{-1})
Spring		17 009	68/69	−563/−420	1.0/0.7	11 118	51/52	−222/−142	0.5/0.3
	Frost	84	39/43	−338/−264	0.9/0.8	256	45/44	−156/−99	0.4/0.3
	Dry	12 246	74/76	−609/−465	1.0/0.7	6508	54/55	−197/−128	0.4/0.2
	Dew	2766	50/50	−454/−323	1.2/0.8	2811	46/46	−222/−144	0.6/0.4
	Rain	1913	54/56	−436/−327	1.0/0.7	1543	52/53	−332/−230	0.8/0.5
Summer		20 340	68/63	−600/−421	1.1/0.7	8416	49/48	−189/−116	0.5/0.3
	Dry	132 554	75/70	−629/−457	1.0/0.7	4571	54/52	−167/−106	0.4/0.2
	Dew	4330	56/52	−566/−360	1.2/0.8	2591	41/39	−183/−101	0.5/0.3
	Rain	2456	49/47	−506/−341	1.2/0.8	1254	46/46	−285/−165	0.7/0.4
Autumn		132 310	38/36	−411/−283	1.4/1.0	13 120	29/27	−184/−114	0.8/0.5
	Frost	54	20/18	−144/−127	0.8/0.7	121	15/13	−78/−54	0.5/0.4
	Dry	8131	43/41	−444/−322	1.3/0.9	6142	30/30	−171/−115	0.8/0.5
	Dew	3303	28/23	−353/−220	1.6/1.2	4328	23/20	−158/−92	0.9/0.6
	Rain	1822	33/32	−378/−258	1.5/1.0	2529	34/35	−265/−173	1.0/0.6
Winter		7935	30/28	−273/−177	1.2/0.8	12 671	29/28	−166/−91	0.7/0.4
	Frost	1198	22/17	−196/−132	1.3/0.8	2241	20/14	−106/−53	0.6/0.4
	Dry	4015	32/31	−297/−194	1.2/0.7	5592	30/29	−163/−92	0.7/0.4
	Dew	1597	27/24	−229/−152	1.2/0.8	2811	28/25	−152/−86	0.8/0.4
	Rain	1125	35/35	−333/−213	1.2/0.8	2027	40/40	−264/−165	0.8/0.5
Total		582 594	56/53	−502/−343	1.1/0.8	45 325	38/37	−189/−114	0.7/0.4

nighttime respectively. Highest v_d were obtained during autumn (1.4 and 0.8 cm s^{-1}, for daytime and nighttime respectively).

Ozone fluxes peaked at noon with maximum deposition fluxes of ± −0.7/−0.8 μg m^{-2} s^{-1} during the spring and the summer (Fig. 2B). During autumn and winter, F values reached maxima of −0.5 and −0.3 μg m^{-2} s^{-1}, respectively. In contrast to F, O_3 concentrations exhibited maxima in the afternoon for all considered seasons. Half-hourly F values and O_3 concentrations were weakly correlated ($R^2 = 0.10$). Maximal values of v_d were reached in the morning (data not shown).

Measured F values differed significantly among canopy wetness categories (Table 1) but there was a considerable impact of time of the day on magnitude of the flux. During the day, highest deposition fluxes were generally measured for a dry canopy, which was connected with higher O_3 concentrations compared to the other categories. During the winter, there was no significant difference in F and O_3 concentrations between a rain-wetted and a dry canopy. Smallest deposition fluxes were measured for a dew-wetted canopy and when frost conditions prevailed. At night, a rain-wetted canopy proved to be the best sink for O_3, although concentrations were not significantly higher compared to a dry canopy. For a dry canopy, the ozone sink was only 60% of that from a rain-wetted canopy.

Ozone flux partitioning

Daily O_3 concentrations reached maximum levels (of 70–90 μg m^{-3}) during the period May–July (day of year, DOY 125–210) although there was a high variability (illustrated by high standard errors) (Fig. 3A). Daily O_3 concentrations were better correlated with global radiation (R_g, $R^2 = 0.77$) than with temperature (T) or vapour pressure deficit (vpd), for which R^2 was 0.60 and 0.65, respectively. Measured F, representing the daily ozone uptake by the stand, peaked during the same period (daily maxima of −0.5/−0.6 μg m^{-2} s^{-1}), but the standard errors were larger than in the case of concentrations (Fig. 3B). Measured F values were better correlated with R_g ($R^2 = 0.74$) than with T ($R^2 = 0.60$) or vpd ($R^2 = 0.65$). The course of the daily stomatal ozone flux across the year, based on model results, was more evenly distributed with a peak around DOY 175, when R_g levels were the highest ($R^2 = 0.91$). The daily maxima from the stomatal fluxes during the summer half-year ranged between −0.1 and −0.2 μg m^{-2} s^{-1}. The fraction of the daily stomatal fluxes to the daily measured fluxes (F_s/F) averaged about 20%. The latter fraction was, however, subject to a high seasonal and diurnal variability (Fig. 4). Highest F_s/F fractions were measured during the summer (28%) and spring (20%), with ratios peaking in the afternoon (38% and 30% respectively). During autumn and winter the F_s/F ratio decreased to 12% and 8% respectively. Lowest F_s/F ratios were reached in the morning hours.

Although the share of F_{ns} decreased during the summer half-year, highest F_{ns} values were still measured during this time of the year. On a daily basis, F_{ns} was correlated with O_3 concentrations ($R^2 = 0.49$), R_g ($R^2 = 0.49$), T ($R^2 = 0.41$) and vpd ($R^2 = 0.40$), which all peaked during the same time of the year.

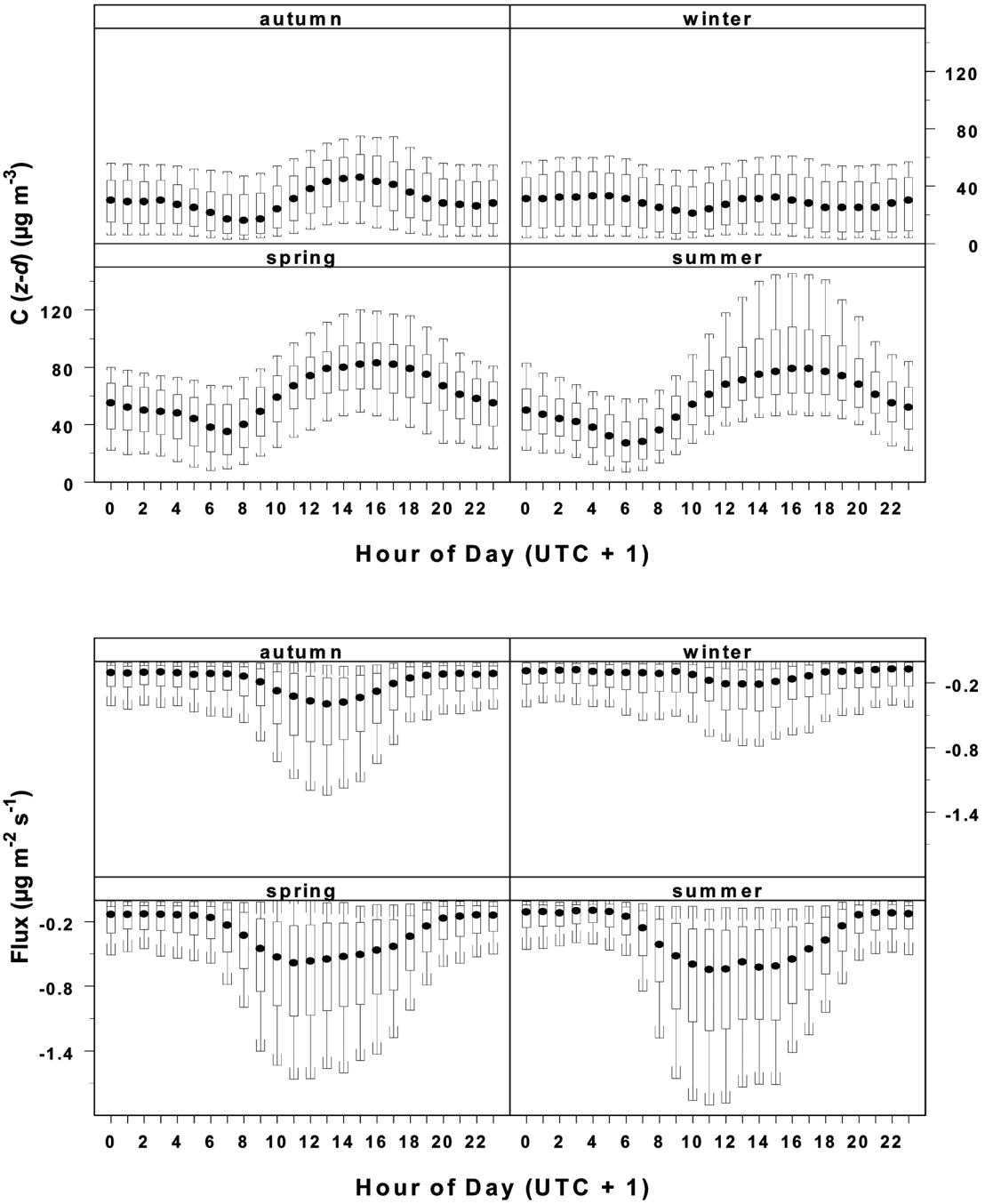

Fig. 2 Seasonal averaged diurnal variability in ozone concentrations (A, top panels) and fluxes (B, lower panels) over the period 2000–2010. Truncated boxplots with median and lower/upper quartiles are shown. Whiskers are drawn to the 10th and 90th percentiles.

AOT40 *versus* POD_1

The annual accumulated ozone exposure over a threshold of 40 ppb (AOT40) at the displacement height varied between 4000 and 15 000 ppb h (Fig. 5). The critical level of 5000 ppb h was exceeded in most of the years. The annual Phytotoxic Ozone Dose (POD_1), obtained from the modelled stomatal ozone fluxes, ranged between 14 and 22 mmol m^{-2} PLA. The critical level of 8 mmol m^{-2} was, therefore, consistently exceeded during the study period. Both indices were positively correlated due to inclusion of O_3 concentrations in the calculation procedure. The explained variability (R^2) ranged between 0.43 (linear function fitting) and 0.70 (in the case of a $\log_{10}$ function fitting).

Variability in non-stomatal resistance (R_{ns})

The long-term geometrical mean R_{ns} of the selected dataset was 136 s m^{-1}, with nighttime values being consistently higher (193 s m^{-1}) than daytime values (102 s m^{-1}) (Table 2). The canopy sink strength was mainly regulated by the non-stomatal pathway, which shortcuts the stomatal sink, given higher values of $R_s(O_3)$. R_{ns} values mostly exceeded the sum of the aerodynamic

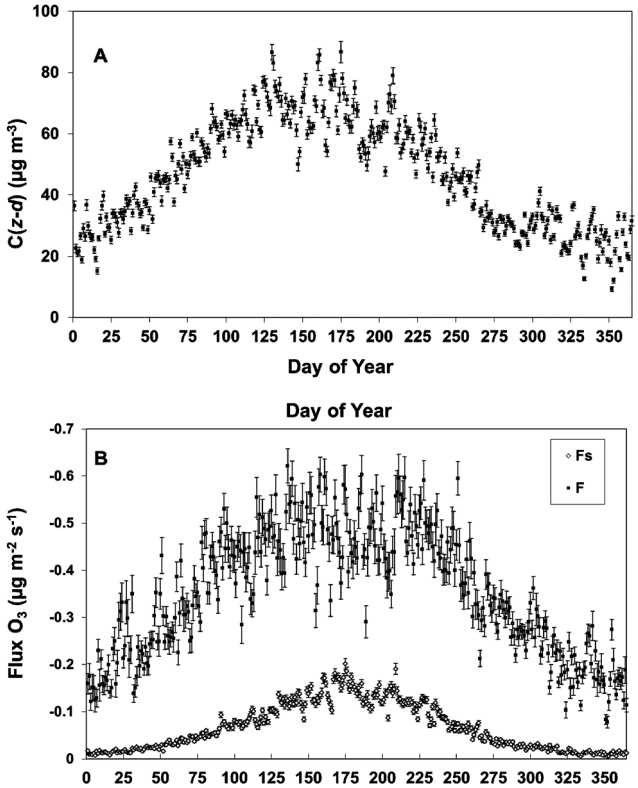

Fig. 3 A (top panel): daily averages of O_3 concentrations at the measuring height ($C(z - d)$) averaged for the period 2000–2010. B (bottom panel): daily averages of stomatal and total measured O_3 fluxes averaged over the period 2000–2010. Standard errors ($n = 9$) around the mean are shown by the vertical bars. F_s = stomatal ozone flux, F = total ozone flux.

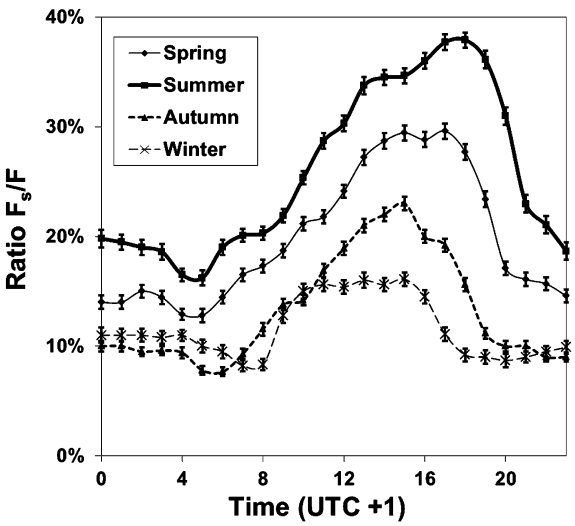

Fig. 4 Seasonally averaged diurnal variability in the ratio of stomatal flux (F_s) to measured flux (F). Standard errors around the mean are shown by the small vertical bars ($n = 550$).

resistance (R_a) and the quasi-laminar boundary layer resistance (R_b), which averaged 45/50 and 25/30 s m^{-1} for nighttime and daytime, respectively. The vertical transfer of ozone was therefore mainly controlled by non-stomatal reactions.

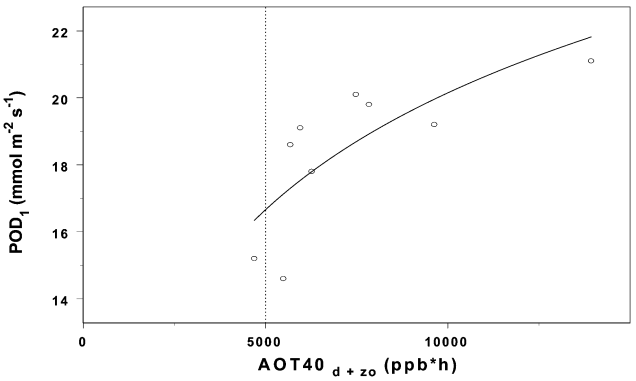

Fig. 5 Relationship between annual concentration-based index AOT40 at the displacement height $d + z_0$ and the flux-based Phytotoxic Ozone Dose (POD_1) for the period 2000–2010 ($n = 9$) using a $\log_{10}$ curve fitting. Critical level of 5000 ppb h shown as dashed line.

The non-stomatal resistance showed a large diurnal variation with lowest values occurring in the morning hours, when turbulence took off (Fig. 6). The diurnal variation was more explicit during the spring and summer. There was also a considerable variation in R_{ns} among the months, especially during nighttime, with lower R_{ns} values being measured during autumn and winter (Fig. 7 and Table 2). This was consistent with the behaviour of the friction velocity ($u*$) at our site, which showed much higher nighttime $u*$ values (more mechanically generated turbulence) during the dormant season (Fig. 7). The monthly variation during the day was far less explicit, both in R_{ns} and $u*$. In order to verify other relationships with environmental variables such as vpd, R_g and T, a principal component analysis was conducted on half-hourly data of R_{ns}, R_g, $u*$, T and vpd. This analysis revealed that for both daytime as well as nighttime, R_{ns} and $u*$ obtained highest loadings along the second PCA-axis, whereas T, vpd and R_g were especially clustered along the first PCA-axis (Table 3). This suggested that the role of $u*$ as the driver of R_{ns} was more important than other variables.

The non-stomatal sink might also depend on the presence of nitric oxide (NO) or BVCOs, which are involved in gas-phase reactions with O_3. A Spearman rank correlation analysis showed that R_{ns} was negatively correlated with nitric oxide (NO) ($r = -0.40$, $p < 0.0001$). The inverse relationship between NO and R_{ns} implied that high NO values led to increased scavenging of ozone (Fig. 8). Data of BVOCS were lacking.

The impact of the canopy wetness on R_{ns} was most distinct during spring and summer nights, when medians and geometric means of R_{ns} exhibited the largest values (Table 2 and Fig. 7). Largest R_{ns} values were noticed for a dry canopy and during spring frost conditions with median and geometric means varying between 300 and 400 s m^{-1}. Rain-wetted canopies constituted the best nighttime non-stomatal sinks ($R_{ns} < 200$ s m^{-1}). During the daytime the role of the canopy wetness was less evident and during spring and winter, no significant differences could be found.

Discussion

Total ozone fluxes

The long-term average ozone flux onto our mixed forest amounted to -366 ng m^{-2} s^{-1}, which nearly equalled the 5 year

Table 2 Summary statistics of long-term averaged friction velocity (u_*) and non-stomatal resistance (R_{ns}) for different canopy wetness categories and time of day (μ_a = arithmetic average, μ_m = median, μ_g = geometric mean, σ_a = standard deviation, σ_g = geometric standard deviation)

		u_*						R_{ns}					
		Daytime			Nighttime			Daytime			Nighttime		
		μ_a	μ_m	σ_a	μ_a	μ_m	σ_a	μ_m	μ_g	σ_g	μ_m	μ_g	σ_g
Spring	Frost	0.46	0.50	0.21	0.38	0.38	0.20	110	124	3	343	393	4
	Dry	0.66	0.66	0.28	0.45	0.40	0.27	117	128	4	296	331	5
	Dew	0.56	0.52	0.30	0.44	0.36	0.29	94	100	5	210	221	4
	Rain	0.70	0.64	0.36	0.59	0.53	0.33	111	116	5	148	149	4
Summer	Dry	0.57	0.56	0.25	0.38	0.30	0.25	112	121	5	342	382	5
	Dew	0.48	0.44	0.26	0.30	0.23	0.21	86	93	5	213	229	5
	Rain	0.55	0.51	0.27	0.45	0.41	0.24	106	106	5	166	173	5
Autumn	Frost	0.44	0.41	0.21	0.39	0.39	0.23	126	153	3	195	176	3
	Dry	0.61	0.59	0.27	0.52	0.47	0.29	82	88	5	158	163	4
	Dew	0.52	0.46	0.29	0.40	0.34	0.26	55	59	5	111	119	4
	Rain	0.68	0.65	0.33	0.60	0.57	0.32	73	71	5	119	121	5
Winter	Frost	0.50	0.46	0.33	0.45	0.43	0.23	79	82	5	180	184	4
	Dry	0.68	0.65	0.32	0.63	0.60	0.33	95	95	5	159	160	5
	Dew	0.60	0.56	0.31	0.57	0.51	0.33	82	87	5	139	144	5
	Rain	0.83	0.79	0.38	0.84	0.81	0.36	79	88	5	134	138	5
Total		0.60	0.58	0.30	0.50	0.44	0.31	96	102	5	184	193	5

average of −394 ng m^{-2} s^{-1} measured above a Danish Norway spruce canopy[4] using the gradient method. In other long-term flux studies conducted in a Norway spruce forest in Southern Norway[30] or a Scots pine forest in southern Finland,[31] lower fluxes or deposition velocities were reported, likely due to the much lower O_3 concentrations in these regions. Long-term flux measurements in a ponderosa pine plantation in California (USA) using the eddy covariance technique yielded 40 to 50% lower fluxes.[5,32] The relatively high ozone deposition at our site could to a large extent be attributed to the presence of substantial nocturnal ozone deposition and deposition during the dormant season, increasing the long-term average.

There was a marked difference in the diurnal variability in ozone fluxes and concentrations. The latter reached highest levels in the afternoon whereas fluxes peaked at noon. The diurnal variation in the ozone fluxes across the four seasons depended as such not only on the diurnal dynamics in stomatal conductance, global radiation or atmospheric turbulence, which all typically peak at noon, but also on ozone levels and especially the canopy sink strength, which reached maximum values in afternoon and morning, respectively, causing the diurnal variation in the ozone uptake. A similar diurnal behaviour in concentrations and fluxes was observed in other flux studies over conifers.[4,5,33,34] According to these studies, the time lag between the maxima of ozone concentrations and stomatal aperture limits the ozone stress during the period of the day with highest stomatal aperture. The temporal disconnects, found at our site, do not necessarily imply that the Scots pine trees may not suffer undue ozone injury. Since

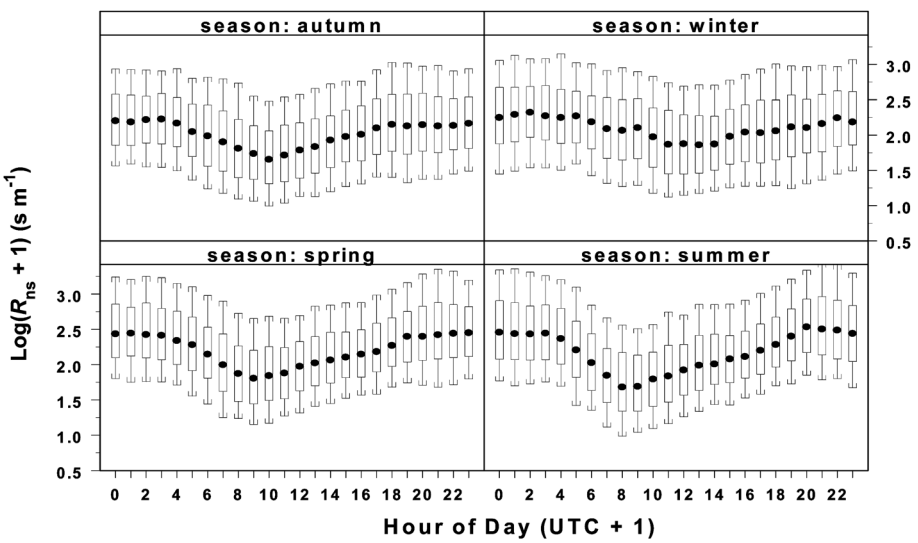

Fig. 6 Diurnal variability in log-transformed non-stomatal resistance (R_{ns}) over the four seasons averaged for the period 2000–2010. Truncated boxplots with median and lower/upper quartile are being shown. Whiskers are drawn to the 10th and 90th percentiles.

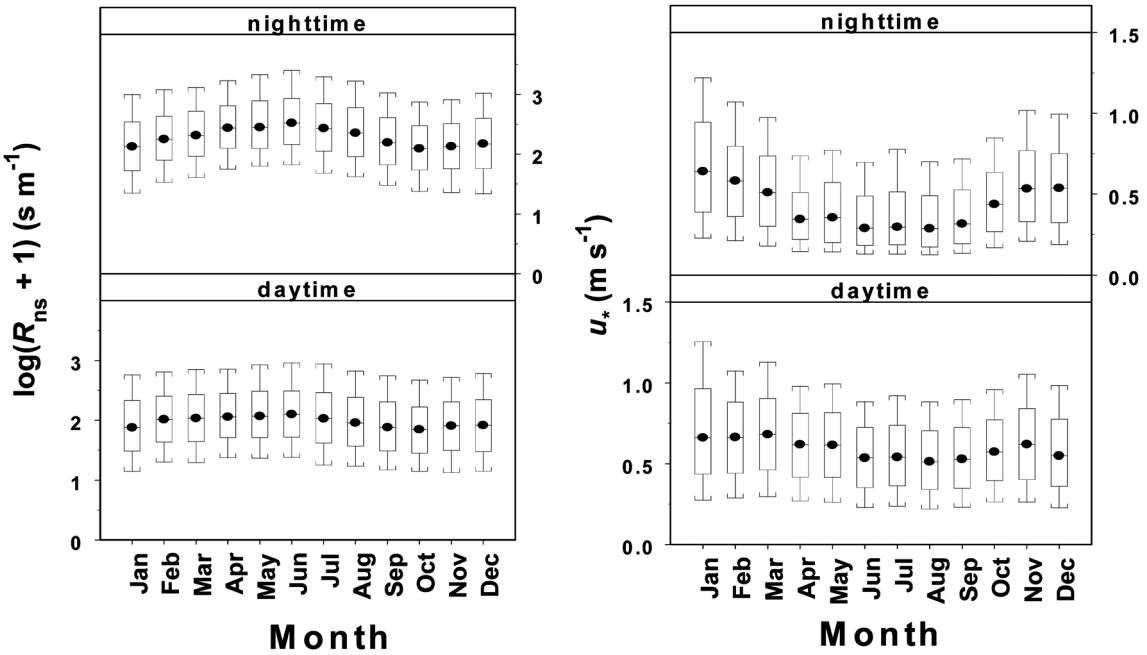

Fig. 7 Monthly variability in log transformed non-stomatal resistance (R_{ns}) for day- and nighttime (left) and monthly variability in friction velocity (u_*) for day- and nighttime. Truncated boxplots with median and lower/upper quartiles are shown. Whiskers are drawn to the 10th and 90th percentiles.

the model did not account for stomatal sluggishness,[35] it could be possible that delayed stomatal aperture occurred due to previous exposure to high ozone concentrations. Hence, ozone uptake could be underestimated in the afternoon hours. Furthermore, no evidence is available that the ozone detoxification capacities of the Scots pine are subject to diurnal variations at our site.

Stomatal *versus* non-stomatal sinks

Stomatal fluxes accounted only for about 20% of the total ozone flux on a multi-year basis, with highest relative stomatal uptake during summer (28%). This proportion was in line with long-term flux measurements of Mikkelsen and colleagues[4] over a Danish Norway spruce stand, for which the proportion of stomatal uptake was at least 21%. They also found that stomata contributed proportionally more to the ozone deposition during summer (31%). Two-year flux measurements over a Scots pine forest in southern Finland[36] revealed that the stomatal contribution to the total canopy sink was 40% (dry canopy) or smaller (moist conditions). During the 6 years of flux measurements over ponderosa pine, stomatal uptake accounted for 57% of the total fluxes.[5] In contrast to our results, the proportion of stomatal uptake decreased during the summer (towards 30%), which was connected to the predominance of emitted biogenic volatile organic compounds (BVOCs) in the ozone scavenging processes at their site.[5] These non-stomatal processes were strongly temperature dependent and peaked during the summer–autumn period. During winter, however, non-stomatal sinks were almost completely depressed.

Other flux partitioning studies conducted in forest ecosystems were mainly focused on campaigns during the growing season.[34,37–41] Results of these studies confirmed that the stomatal uptake proportion of the total uptake might be highly variable

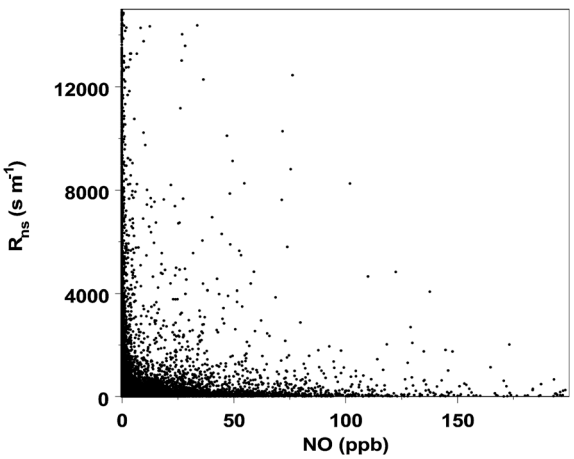

Fig. 8 Relationship between half-hourly concentration of NO (ppb) and non-stomatal resistance (R_{ns}) (in s m^{-1}).

Table 3 Loadings of environmental variables (vpd: vapour pressure deficit, T: temperature, u_*: friction velocity, R_g: global radiation) and non-stomatal resistance (log (R_{ns} + 1)) on PCA-axes during daytime and nighttime conditions

	Daytime		Nighttime	
	PCA axis 1	PCA axis 2	PCA axis 1	PCA axis 2
Variance explained (%)	45	20	41	27
log (R_{ns} + 1)	0.09	−0.77	−0.32	0.60
vpd	0.61	−0.10	−0.67	−0.21
T	0.57	−0.12	−0.65	−0.26
u_*	0.11	0.56	0.17	−0.73
R_g	0.54	0.26	—	—

across study sites. Stomatal uptake comprised 47% of the total flux in a Czech Norway spruce forest.[34] It accounted for 59% of the total uptake in a subalpine pine forest in southern Wyoming (USA).[39] In a similar subalpine forest in the Colorado Rocky Mountains, 81% of the daytime O_3 uptake was predicted to occur through the stomata.[41] Other authors found stomatal fluxes to be responsible for respectively 32% and 51% of the total fluxes in a Holm oak[37] and mixed Holm/Cork oak[38] forest in Central Italy. In a northern mixed hardwood forest in northern Michigan (USA), the summer proportion of the stomatal flux was found to be only 37%.[40]

The low F_s/F fraction at our site could be connected with the extremely low LAI value for our forest, which ranges between 1 and 1.5.[27] This could have resulted in more mixing within the (sub)canopy and hence, more non-stomatal deposition. However, when LAI's of forests from previous studies (previous paragraph) are plotted against their respective fractions, no distinct relationship could be found. The effect of higher LAI's on stomatal uptake could have been partly offset by a higher proportion of sunshaded leaves, leading to decreased stomatal conductances deeper in the dense canopy. It is also conceivable that other factors, such as pollution climate and tree species or age, overrule the impact of LAI.

Metrics for ozone risk assessment

An effort was made to compare the annual ozone dose, expressed by the POD_1 (ICP Vegetation, 2010), with the AOT40 metric based on accumulation of concentrations (UBA, 1996). It was found that a curvilinear fitting procedure was more appropriate to relate the flux-based risk with the exposure based metric. This implied that at high AOT40 values, the Phytotoxic Ozone Dose might not keep track with the rise in the exposure to ozone concentrations, expressed by the AOT40 metric. Given the fact that a flux-based approach is generally considered to be more sound compared to the AOT40 approach, the use of the latter metric may result in overestimates of the risk for ozone exposure. Flux-based risk maps correlated better with observed plant damage.[42] There is now a general consensus that this approach is biologically a more sound procedure to assess the risk for ozone damage.[13,15,43]

The annual values of POD_1 ranged between 14 and 22 mmol m^{-2}, which largely exceeded the critical level of 8 mmol m^{-2}, suggested by ICP Vegetation (2010). The latter was adopted from Norway spruce, based on dose–effect relationships by Karlsson and colleagues[44] (2007). To our knowledge, no specific critical levels have been proposed for Scots pine. Among pine trees, Scots pine is classified as sensitive to ozone damage.[45]

Drivers of non-stomatal sinks

Ozone fluxes were largely controlled by non-stomatal sinks (geometric mean of 136 s m^{-1}), with daytime R_{ns} being two times lower than the nighttime values. The nighttime R_{ns} values and also the values recorded during wintertime were low enough, compared to the canopy stomatal resistance, to allow for substantial ozone deposition when the physiological activity of the pine trees was low, which was also observed in other studies.[4,46]

The non-stomatal sink strength showed a large diurnal and seasonal variation. Lowest values of R_{ns} were obtained in the morning hours and during autumn. These diurnal and seasonal dynamics were likewise followed by v_d, due to the fact that R_{ns} was the most determinant resistance in the total resistance (R_t) of the vertical transfer (eqn (4)). Morning dips of R_{ns}, as low as 60 s m^{-1}, were also observed by Gerosa and colleagues[37] in a Mediterranean oak forest during dry summer and mild autumn conditions. Just as at our site it was suggested that the high affinity of the non-stomatal sink in the morning could be connected with the onset of turbulence. Due to enhanced mixing of air layers, ozone is entrained from above the canopy into the trunk/canopy space where it reacts with stored NO.[47] Other flux studies in forests reported that R_{ns} exhibited a diel behaviour reaching a minimum during midday periods.[5,40,48–50] Such a behaviour was similar to the diurnal cycle of global radiation and lent support to the hypothesis of ozone destroying photochemical processes at the cuticle surface.[48] The apparent effect of global radiation on the non-stomatal flux might also reflect thermal decomposition of O_3 at the canopy surface.[51] Also emission maxima of many monoterpenes in coniferous forests have been used as evidence in explaining enhanced non-stomatal deposition at noon.[5,52–54]

Non-stomatal processes can be subdivided by the loss of O_3 on plant (soil) surfaces or reactions with molecules such as nitric oxide (NO) or BVOCs in the canopy space, or above.[55] According to Rondon and colleagues,[48] non-stomatal processes followed a complex mechanism in which several factors such as light intensity, temperature, humidity and chemical properties of the cuticle surface are involved. The role of wetness or relative humidity in enhancing the non-stomatal O_3 flux has been amply demonstrated in other studies.[36,41,56–59] Altimir and colleagues[36] suggested that chemical reactions of O_3 at the surface were modulated by water films on the surface. Other authors suggested that rainfall after drought periods enhanced the formation of BVOCs.[41,52] Also the presence of dew at night and during the morning was found to enhance ozone deposition in a maritime pine forest, which might be explained by the presence of dissolved chemical species in water.[56] At our site the impact of canopy wetness was the most explicit during the spring and summer nights. Rain-wetted canopies constituted the best nighttime non-stomatal sinks (R_{ns} < 200 s m^{-1}). The high sink strength of rain-wetted canopies could be due to relatively higher friction velocities and hence, better mixing conditions compared to dew-wetted canopies (Table 2).[60,61]

A principal component analysis selected friction velocity as the main environmental variable controlling the non-stomatal sink at our site. Turbulent mixing processes were also identified as important drivers in enhancing non-stomatal O_3 deposition at other forest sites.[56,60,62] Enhanced mixing could bring emitted BVOCs and NO, present in the trunk or canopy space, in contact with O_3. At higher u_* a larger fraction of the canopy area would also become available for deposition. At our site the behaviour of u_* can explain the decreased R_{ns} during the morning and the large difference in (nocturnal) R_{ns} between the dormant and growing season. The lower R_{ns}, measured during autumn, was in line with observations over a Norway spruce forest in North-eastern Bavaria (Germany).[63] The latter authors found a temporal trend in the cuticular resistance, with an average value of 440 s m^{-1} at

the beginning of May, dropping to values of 180 s m^{-1} at the end of October.

Highest non-stomatal deposition was measured during the growing season, which might be due to higher O_3 levels and more intense cuticle or gas-phase reactions with BVOCs and NO, due to more elevated T and R_g. The emission of monoterpenes, like α-pinenes, β-pinenes and 3-carenes, typical for pine trees and coniferous forest in general, is temperature-dependent and globally peaks in the summer half-year.[53,54,64] Oxidation products of these reactive terpenes were measured during a summer campaign at our site,[65] which indicated that ozonolysis of terpenes could have been important. The presence of NO-emission at our nitrogen saturated site was evidenced by upward NO_x-fluxes,[18] which annually averages between 0.010 and 0.030 ppb m s^{-1}. Also gas flux measurements from incubated soil and forest floor samples indicated the presence of NO emission.[66] Nitric oxide was found to be emitted from forest floor samples at a rate of ±300 μg N m^{-2} h^{-1} (at ambient moisture content). Emission of NO is claimed to be important at coniferous sites, especially those which are nitrogen saturated.[67] Also the advanced acidification state of the site[68] could have exacerbated NO losses during chemical processes.[69] We speculate that NO emission is the main driver for the non-stomatal reactions, because of the explicit inverse relationship between R_{ns} and NO. If gas-phase reactions were ruled by scavenging of O_3 by BVOCs, R_{ns} would reach minimum levels at noon, rather than in the early morning. In addition, NO will react more readily with O_3 as compared to BVOCs in the trunk and sub-canopy space, as was shown in a study of O_3 deposition at a nitrogen saturated Douglas fir stand in the Netherlands.[47]

Conclusions

O_3 was highly reactive at the site (v_d = 9 mm s^{-1}) and the deposition was largely controlled by non-stomatal processes. The non-stomatal sinks accounted for 80% of the total ozone fluxes but the portion of non-stomatal fluxes was subject to a high diurnal and seasonal variability.

The current lack of knowledge about non-stomatal processes in forests might be responsible for substantial model underestimates of O_3 losses over forested surfaces. Ozone deposition is known to be enhanced over forest canopies because of increased turbulence. The sink strength is, however, highly variable and all possible pathways should be taken into account to quantify the overall removal of tropospheric O_3 by forest vegetation. The EMEP model currently assumes that the non-stomatal sink is only passively scavenging O_3, with a low and constant resistance. It is clear, however, that non-stomatal pathways should be further scrutinized.

Acknowledgements

This project was performed under the authority of the Flemish Minister of the Environment. We gratefully acknowledge the Flemish Environmental Agency (VMM) for the continuous support in the calibration of the monitors. Further support was provided by the Carbo-Europe Integrated Project of the European Commission. We are indebted to expert Eddy Smesman for the meticulous maintenance of the tower and its instruments, as well as to Fred Kockelbergh (University of Antwerp) for the maintenance of the sonic anemometer at the site. The authors gratefully acknowledge the work of Dr M. Op De Beeck in the stomatal conductance modelling.

References

1 M. R. Ashmore, *Plant, Cell Environ.*, 2005, **28**, 949–964.
2 D. Fowler, K. Pilegaard, M. A. Sutton, P. Ambus, M. Raivonen, J. Duyzer, D. Simpson, H. Fagerli, S. Fuzzi, J. K. Schjoerring, C. Granier, A. Neftel, I. S. A. Isaksen, P. Laj, M. Maione, P. S. Monks, J. Burkhardt, U. Daemmgen, J. Neirynck, E. Personne, R. Wichink-Kruit, K. Butterbach-Bahl, C. Flechard, J. P. Tuovinen, M. Coyle, G. Gerosa, B. Loubet, N. Altimir, L. Gruenhage, C. Ammann, S. Cieslik, E. Paoletti, T. N. Mikkelsen, H. Ro-Poulsen, P. Cellier, J. N. Cape, L. Horvath, F. Loreto, U. Niinemets, P. I. Palmer, J. Rinne, P. Misztal, E. Nemitz, D. Nilsson, S. Pryor, M. W. Gallagher, T. Vesala, U. Skiba, N. Brueggemann, S. Zechmeister-Boltenstern, J. Williams, C. O'Dowd, M. C. Facchini, G. de Leeuw, A. Flossman, N. Chaumerliac and J. W. Erisman, *Atmos. Environ.*, 2009, **43**, 5193–5267.
3 R. C. Wilson, Z. L. Fleming, P. S. Monks, G. Clain, S. Henne, I. B. Konovalov, S. Szopa and L. Menut, *Atmos. Chem. Phys. Discuss.*, 2011, **11**, 18433–18485.
4 T. N. Mikkelsen, H. Ro-Poulsen, M. F. Hovmand, N. O. Jensen, K. Pilegaard and A. H. Egeløv, *Atmos. Environ.*, 2004, **38**, 2361–2371.
5 S. Fares, M. Mckay, R. Holzinger and A. H. Goldstein, *Agric. Forest Meteorol.*, 2010, **150**, 420–431.
6 J. N. Cape, *Sci. Total Environ.*, 2008, **400**, 257–269.
7 D. Fowler, J. N. Cape, M. Coyle, C. Flechard, J. Kuylenstierna, K. Hicks, D. Derwent, C. Johnson and D. Stevenson, *Water, Air, Soil Pollut.*, 1999, **116**, 5–32.
8 J. R. Dorsey, J. H. Duyzer, M. W. Gallagher, H. Coe, K. Pilegaard, J. G. Weststrate, N. O. Jensen and S. Walton, *Q. J. R. Meteorol. Soc.*, 2004, **130**, 1941–1955.
9 A. Bytnerowicz, K. Omasa and E. Paoletti, *Environ. Pollut.*, 2007, **147**, 438–445.
10 P. J. Hanson, S. D. Wullschleger, R. J. Norby, T. J. Tschaplinski and C. A. Gunderson, *Global Change Biol.*, 2005, **11**, 1402–1423.
11 M. Lindner, M. Maroschek, S. Netherer, A. Kremer, A. Barbati, J. Garcia-Gonzalo, R. Seidl, S. Delzon, P. Corona, M. Kolstrom, M. J. Lexer and M. Marchetti, *Forest Ecol. Manage.*, 2010, **259**, 698–709.
12 S. V. Ollinger, J. D. Aber, P. B. Reich and R. J. Freuder, *Global Change Biol.*, 2002, **8**, 545–562.
13 S. A. Cieslik, *Atmos. Environ.*, 2004, **38**, 2409–2420.
14 E. Paoletti and W. J. Manning, *Environ. Pollut.*, 2007, **150**, 85–95.
15 R. Matyssek, A. Bytnerowicz, P. E. Karlsson, E. Paoletti, M. Sanz, M. Schaub and G. Wieser, *Environ. Pollut.*, 2007, **146**, 587–607.
16 J. P. Tuovinen, L. Emberson and D. Simpson, *Ann. Forest Sci.*, 2009, **66**, 401.
17 J. Klingberg, M. Engardt, J. Uddling, P. E. Karlsson and H. Pleijel, *Tellus A*, 2011, **63**, 174–187.
18 J. Neirynck, A. S. Kowalski, A. Carrara, G. Genouw, P. Berghmans and R. Ceulemans, *Environ. Pollut.*, 2007, **149**, 31–43.
19 A. J. Dyer and B. B. Hicks, *Q. J. R. Meteorol. Soc.*, 1970, **96**, 715–721.
20 J. A. Businger, J. C. Wyngaard, Y. Izumi and E. F. Bradley, *J. Atmos. Sci.*, 1971, **28**, 181–189.
21 F. C. Bosveld, Exchange Coefficients Over a Douglas Fir Forest, Dutch Priority Programme on Acidification, WR-91-02, Royal Netherlands Meteorological Institute (KNMI), De Bilt, 1991.
22 A. S. O. A. M. Monin, *Basic Laws of Turbulence Mixing in the Ground Layer of the Atmosphere*, Academy Nauk SSSR, Trudii Geo Phisical Institut, 1954, vol. 24, pp. 163–187.
23 J. A. Garland, *Atmos. Environ.*, 1978, **12**, 349–362.
24 A. C. L. Beljaars and A. A. M. Holtslag, *Environmental Software*, 1990, **5**, 60–68.
25 B. B. Hicks, D. D. Baldocchi, T. P. Meyers, R. P. Hosker and D. R. Matt, *Water, Air, Soil Pollut.*, 1987, **36**, 311–330.
26 G. Gerosa, M. Vitale, A. Finco, F. Manes, A. B. Denti and S. Cieslik, *Atmos. Environ.*, 2005, **39**, 3255–3266.

27 M. Op de Beeck, B. Gielen, I. Jonckheere, R. Samson, I. A. Janssens and R. Ceulemans, *Biogeosciences*, 2010, **7**, 199–215.
28 G. D. Farquhar, S. V. Caemmerer and J. A. Berry, *Planta*, 1980, **149**, 78–90.
29 R. Leuning, *Plant, Cell Environ.*, 1995, **18**, 339–355.
30 L. R. Hole, A. Semb and K. Tørseth, *Atmos. Environ.*, 2004, **38**, 2217–2223.
31 P. Keronen, A. Reissell, U. Rannik, T. Pohja, E. Siivola, V. Hiltunen, P. Hari, M. Kulmala and T. Vesala, *Boreal Environ. Res.*, 2003, **8**, 425–443.
32 M. R. Kurpius, M. Mckay and A. H. Goldstein, *Atmos. Environ.*, 2002, **36**, 4503–4515.
33 N. Altimir, J. Tuovinen, T. Vesala, M. Kulmala and P. Hari, *Atmos. Environ.*, 2004, **38**, 2387–2398.
34 M. Zapletal, P. Cudlin, P. Chroust, O. Urban, R. Pokorny, M. Edwards-Jonasova, R. Czerny, D. Janous, K. Taufarova, Z. Vecera, P. Mikuska and E. Paoletti, *Environ. Pollut.*, 2011, **159**, 1024–1034.
35 E. Paoletti and N. E. Grulke, *Environ. Pollut.*, 2010, **158**, 2664–2671.
36 N. Altimir, P. Kolari, J. P. Tuovinen, T. Vesala, J. Back, T. Suni, M. Kulmala and P. Hari, *Biogeosciences*, 2006, **3**, 209–228.
37 G. Gerosa, M. Vitale, A. Finco, F. Manes, A. B. Denti and S. Cieslik, *Atmos. Environ.*, 2005, **39**, 3255–3266.
38 S. Cieslik, *Environ. Pollut.*, 2009, **157**, 1487–1496.
39 K. F. Zeller and N. T. Nikolov, *Environ. Pollut.*, 2000, **107**, 1–20.
40 A. Hogg, J. Uddling, D. Ellsworth, M. A. Carroll, S. Pressley, B. Lamb and C. Vogel, *Tellus, Ser. B*, 2007, **59**, 514–525.
41 A. A. Turnipseed, S. P. Burns, D. J. P. Moore, J. Hu, A. B. Guenther and R. K. Monson, *Agric. Forest Meteorol.*, 2009, **149**, 1447–1459.
42 F. Hayes, M. L. M. Jones, G. Mills and M. Ashmore, *Environ. Pollut.*, 2007, **146**, 754–762.
43 M. Ferretti, F. Bussotti, V. Calatayud, M. Schaub, N. Krauchi, B. Petriccione, G. Sanchez-Pena, M. J. Sanz and E. Ulrich, *Environ. Pollut.*, 2007, **145**, 652–655.
44 P. E. Karlsson, L. Tang, J. Sundberg, D. Chen, A. Lindskog and H. Pleijel, *Environ. Pollut.*, 2007, **150**, 96–106.
45 A. M. Townsend and L. S. Dochinger, Relative sensitivity of pine species to ozone, *J. Arboric.*, 1982, **8**, 186–188.
46 K. Pilegaard, N. O. Jensen and P. Hummelshoj, *Water, Air, Soil Pollut.*, 1995, **85**, 2223–2228.
47 J. H. Duyzer, J. R. Dorsey, M. W. Gallagher, K. Pilegaard and S. Walton, *Q. J. R. Meteorol. Soc.*, 2004, **130**, 1957–1971.
48 A. Rondon, C. Johansson and L. Granat, *J. Geophys. Res.*, 1993, **98**, 5159–5172.
49 L. Granat and A. Richter, *Atmos. Environ.*, 1995, **29**, 1677–1683.
50 H. Coe, M. W. Gallagher, T. W. Choularton and C. Dore, *Atmos. Environ.*, 1995, **29**, 1413–1423.
51 D. Fowler, C. Flechard, J. N. Cape, R. L. Storeton-West and M. Coyle, *Water, Air, Soil Pollut.*, 2001, **130**, 63–74.
52 R. Holzinger, A. Lee, M. Mckay and A. H. Goldstein, *Atmos. Chem. Phys.*, 2006, **6**, 1267–1274.
53 A. H. Goldstein, M. Mckay, M. R. Kurpius, G. W. Schade, A. Lee, R. Holzinger and R. A. Rasmussen, *Geophys. Res. Lett.*, 2004, **31**, 1–4.
54 C. Holzke, T. Hoffmann, L. Jaeger, R. Koppmann and W. Zimmer, *Atmos. Environ.*, 2006, **40**, 3174–3185.
55 J. N. Cape, R. Hamilton and M. R. Heal, *Atmos. Environ.*, 2009, **43**, 1116–1123.
56 E. Lamaud, A. Carrara, Y. Brunet, A. Lopez and A. Druilhet, *Atmos. Environ.*, 2002, **36**, 77–88.
57 J. D. Fuentes, T. J. Gillespie, G. Denhartog and H. H. Neumann, *Agric.Forest Meteorol.*, 1992, **62**, 1–18.
58 G. Gerosa, A. Finco, S. Mereu, R. Marzuoli and A. Ballarin-Denti, *Biogeosciences*, 2009, **6**, 1783–1798.
59 L. M. Zhang, M. D. Moran, P. A. Makar, J. R. Brook and S. L. Gong, *Atmos. Environ.*, 2002, **36**, 537–560.
60 L. Zhang, J. R. Brook and R. Vet, *Atmos. Chem. Phys.*, 2003, **3**, 2067–2082.
61 L. M. Zhang, J. R. Brook and R. Vet, *Atmos. Environ.*, 2002, **36**, 4787–4799.
62 K. Matsuda, I. Watanabe and V. Wingpud, *Atmos. Environ.*, 2005, **39**, 2571–2577.
63 O. Klemm and A. Mangold, *Water, Air, Soil Pollut.: Focus*, 2001, **1**, 223–232.
64 R. W. Janson, *J. Geophys. Res.*, 1993, **98**, 2839–2850.
65 Y. Gomez-Gonzalez, W. Wang, R. Vermeylen, X. Chi, J. Neirynck, I. A. Janssens, W. Maenhaut and M. Claeys, *Atmos. Chem. Phys. Discuss.*, 2011, **11**, 23541–23572.
66 D. Wagner, *Climate Change Effects on Greenhouse Gas Emissions from Northern European Soils*, Diplomstudium Theoret./ Angewandte Geographie, University of Wien, 2009.
67 K. Pilegaard, U. Skiba, P. Ambus, C. Beier, N. Bruggemann, K. Butterbach-Bahl, J. Dick, J. Dorsey, J. Duyzer, M. Gallagher, R. Gasche, L. Horvath, B. Kitzler, A. Leip, M. K. Pihlatie, P. Rosenkranz, G. Seufert, T. Vesala, H. Westrate and S. Zechmeister-Boltenstern, *Biogeosciences*, 2006, **3**, 651–661.
68 J. Neirynck, I. A. Janssens, P. Roskams, P. Quataert, P. Verschelde and R. Ceulemans, *Biogeochemistry*, 2008, **91**, 201–222.
69 R. T. Venterea, P. M. Groffman, L. V. Verchot, A. H. Magill, J. D. Aber and P. A. Steudler, *Global Change Biol.*, 2003, **9**, 346–357.